Period Estimation of an Almost Periodic Signal Using Persistent Homology With Application to Respiratory Rate Measurement

Fatih Erden, *Member, IEEE*, and A. Enis Cetin, *Fellow, IEEE*

***Abstract*—Time-frequency techniques have difficulties in yielding efficient online algorithms for almost periodic signals. We describe a new topological method to find the period of signals that have an almost periodic waveform. Proposed method is applied to signals received from a pyro-electric infrared sensor array for the online estimation of the respiratory rate (RR) of a person. Time-varying analog signals captured from the sensors exhibit an almost periodic behavior due to repetitive nature of breathing activity. Sensor signals are transformed into two-dimensional point clouds with a technique that allows preserving the period information. Features, which represent the harmonic structures in the sensor signals, are detected by applying persistent homology and the RR is estimated based on the persistence barcode of the first Betti number. Experiments have been carried out to show that our method makes reliable estimates of the RR.**

***Index Terms*—Periodicity, persistent homology, pyro-electric infrared (PIR) sensor, respiratory rate (RR), topological data analysis.**

I. Introduction

THERE are many processes that are not strictly periodic but measuring them results in signals of which the shape and period slightly differs over time [1]. Such signals are referred to as *almost periodic* signals. A more formal definition can be found in [2]. Time-frequency techniques have difficulties in yielding effective and consistent online algorithms for almost periodic signals because of the inherent nonstationarity as discussed in [3] and [4]. On the other hand, topological data analysis (TDA) can be a powerful tool to overcome some of these difficulties and offer a reliable alternative.

In this study, a set of TDA tools are employed to extract period information from a given almost periodic signal. The signal is first transformed into a two-dimensional (2-D) point cloud. Point clouds are usually constructed from time-delay embeddings of signals for the analysis of dynamical systems [5]–[7]. In [5], 2-D time-delay embeddings of sound signals are investigated using persistent homology for wheeze detection. In wheeze detection, it is sufficient to determine whether the signal is periodic, that is, there is no need to find the period. Moreover, the 2-D delay-coordinate embedding method loses the temporal period information. It is shown in [8] that it is possible to estimate the frequency of an almost harmonic signal using 3-D delay embeddings. However, this method requires an additional dimension. Instead of using delay embeddings, we propose a new method for 2-D point cloud construction that allows preserving period information of the original signal. Considering that the dc value of the signal is known, we transform each half-cycle of the almost periodic signal to a topological hole by inserting mean-valued samples between every other input sample. Then, we detect the holes in the resulting topological space by persistent homology, and estimate the period of each cycle based on the persistence barcode of the first Betti number. The proposed method, in contrast to many time-frequency techniques, does not require a batch of data for period estimation. The period is estimated whenever a new cycle is detected. Since it is required to wait for a complete cycle to find the period, we regard our method as an *online* method. In addition, since the TDA describes global representations of the objects, it is more robust to missing data points.

Respiratory rate (RR) is one of the most important vital signs in assessing the physical and psychological health of people [9], [10]. RR measurement has been studied in many previous works using a wide variety of techniques [11]–[15]. In this letter, we present a noninvasive pyro-electric infrared (PIR) sensor array-based system. It is similar to the one previously developed in [16] with the difference that accelerometer is now replaced with an extra PIR sensor. Data received from the sensors are processed using the TDA method to estimate the RR. Experiments have been carried out to demonstrate that our method makes reliable measurements of the RR.

The remainder of the letter is organized as follows. Operating principles of a PIR sensor and the multisensor system set-up are described in Section II. Extraction of the point clouds from 1-D PIR sensor signals and their topological characterization are exploited in Section III. Experimental results are presented in Section IV, and finally Section V concludes the letter.

II. PIR Sensors and System Description

PIR sensors are electronic devices designed to sense the motion of subjects within their field of view (FoV). Indeed, rather

Manuscript received March 18, 2017; revised April 26, 2017; accepted April 27, 2017. Date of publication April 27, 2017; date of current version May 10, 2017. This letter was presented in part at the 50th Asilomar Conference on Signals, Systems and Computers, Pacific Grove, CA, USA, November 2016. The associate editor coordinating the review of this manuscript and approving it for publication was Dr. Mehdi Moradi. *(Corresponding author: Fatih Erden.)*

F. Erden is with the Department of Electrical and Electronics Engineering, Bilkent University, Ankara 06800, Turkey (e-mail: erden@ee.bilkent.edu.tr).

A. E. Cetin is with the Department of Electrical and Computer Engineering, University of Illinois at Chicago, Chicago, IL 60607 USA, on leave from the Department of Electrical and Electronics Engineering, Bilkent University, Ankara 06800, Turkey (e-mail: cetin@bilkent.edu.tr).

Color versions of one or more of the figures in this letter are available online at http://ieeexplore.ieee.org.

Digital Object Identifier 10.1109/LSP.2017.2699924

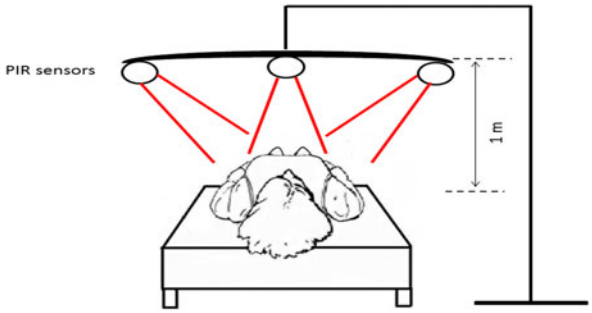

Fig. 1. PIR sensor array-based RR measurement system.

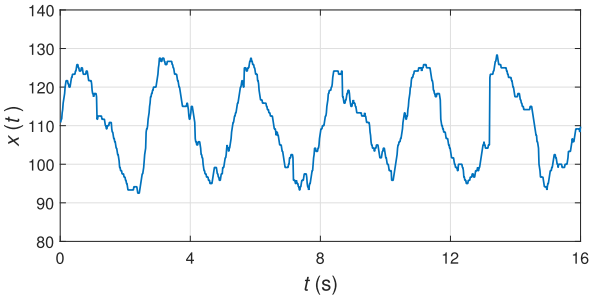

Fig. 2. PIR sensor signal due to normal breathing activity. Sampled at 100 Hz and digitized using 8-bit quantization.

than sensing the motion, a PIR sensor detects the change in the amount of IR radiation impinging upon it. We use a dual-element PIR sensor. It has two pyro-electric elements inside and functions by measuring the difference in IR radiation between these elements. If there are activities from a hot body, a binary "1" is sent to the controller and a binary "0," otherwise. The capability of those sensors are limited to on/off mode operations. However, a continuous-time analog signal, which represents the transient behavior of the sensor circuit, can be captured from the PIR sensor through slight modification of the sensor circuitry as described in [17]. Leveraging this technique, a PIR sensor can provide further definition of the monitored area and individual(s).

The multisensor RR measurement system comprises of three PIR sensors that are located onto a stand near a bed. FoVs of the sensors are narrowed to focus on the separate parts of the chest and hence filter out the lower body movements. Proposed set-up is shown in Fig. 1. Time-varying sensor signals are digitized using an analog-to-digital-converter (ADC) and transferred to a general-purpose computer for further processing. RR for an adult at rest is 12–20 breaths\min (bpm) and increases to 30–50 bpm in an exercise testing [18]. That is, the breathing activity is a low-frequency activity with the highest frequency $\sim$1 Hz, and thus the sensor signal should be sampled at a rate equal to at least 2 Hz. Response of the PIR sensor in the middle, $x(t)$, due to a person lying supine in bed and breathing normally is depicted in Fig. 2. When the person inhales, his chest expands and becomes closer to the PIR sensor; when the person exhales, his chest contracts and moves away from the sensor causing an almost periodic signal.

III. Topological Signal Processing

Topology deals with the intrinsic geometric properties of the objects. The objects in this study are the simplicial complexes

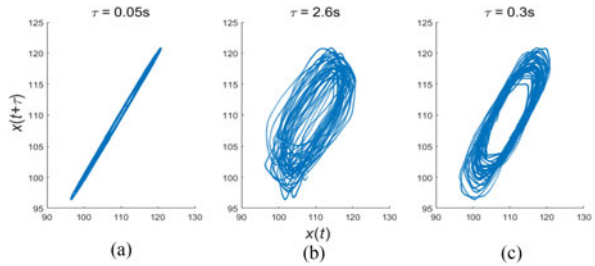

Fig. 3. Point clouds constructed from delay-coordinate embedding of the PIR sensor signal with different τ values.

that will be built over the point clouds. Prior to proceeding with the construction of point clouds, we filter the raw sensor output by a moving average filter. This removes the noise making the harmonic patterns in the breathing signals more conspicuous.

A. From 1-D Signals to Point Clouds

A point cloud is a finite set of points that are equipped with a notion of distance. One way to construct a point cloud for topological analysis of a time-series is to use time-delay coordinate embeddings [5]. Delay-coordinate embedding method defines a multidimensional space where each dimension subsumes a delayed version of the signal [19]. That is, given a time-series $x(t)$ and an embedding dimension m, a vector quantity of m components can be described as follows [3]:

$$X(t) = (x(t), x(t+\tau_1), x(t+\tau_2), \ldots, x(t+\tau_{m-1})) \quad (1)$$

where τ_i is delay constant of the ith dimension. Transformation of a signal for each choice of the delay time and embedding dimension results in a different geometry. Suppose that we construct a point cloud by setting $m = 2$ in (1). If τ is not selected properly, the point cloud may not truly reflect the underlying topology. Two such instances when τ is too small and too high are shown in Fig. 3(a) and (b), respectively. On the other hand, Fig. 3(c) shows the point cloud with τ determined using the autocorrelation method described in [5]. The resulting space exhibits an elliptical structure with a clean hole in the center indicating that the signal is almost periodic.

The only information we can infer from the 2-D delay embeddings is whether the signal is (almost) periodic or not. The period information of the original signal is lost during the transformation. To preserve the period information, we propose another way of constructing a point cloud. Let $x(n)$ be an almost periodic time-series signal for $n = 0, 1, \ldots, N-1$ and μ be the mean value. Notice that μ is the baseline level of the sensor output and known ahead of time. To transform each half-cycle of the oscillatory signal to a topological hole, we insert μ-valued samples between each pair of samples of $x(n)$ to have

$$x' = [x(0), \mu, x(1), \ldots, x(N-2), \mu, x(N-1)]^T \quad (2)$$

and form a 2-D point cloud with the sample indices being the second dimension, that is

$$Z = [x' \quad t] \quad (3)$$

where $t = [0, 1, \ldots, 2(N-1)]^T$. Each row in Z represents the coordinate of a point in the 2-D space. The point cloud constructed in this way is depicted in Fig. 4, where z_1 and z_2 denote the first and second columns of Z, respectively. It now exhibits

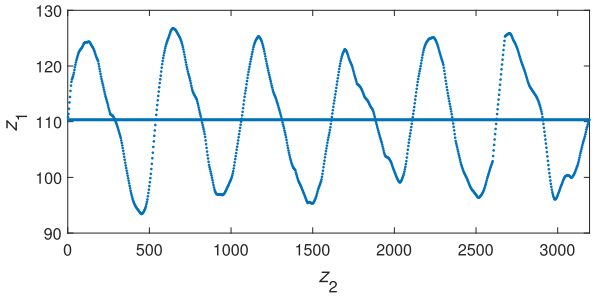

Fig. 4. Point cloud constructed using the proposed method.

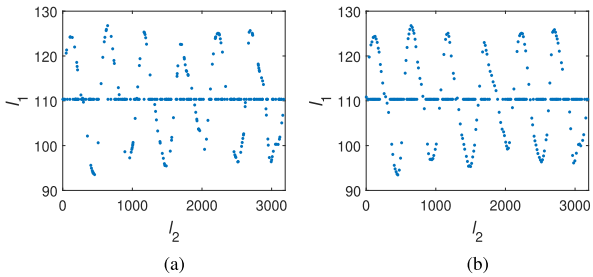

Fig. 5. Point cloud subsampling, (a) randomly and (b) by the maxmin method, with a ratio of ∼10 to 1.

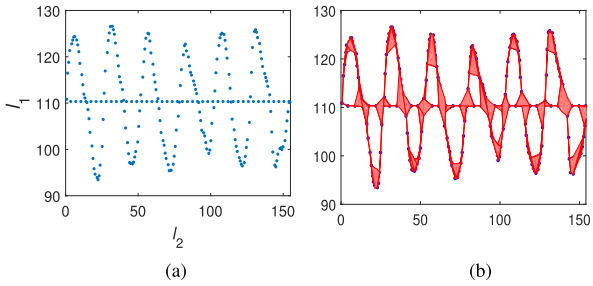

Fig. 6. (a) Point cloud reduced by the proposed technique and (b) the corresponding Vietoris-Rips complex for $r = 6$.

a plurality of semi-elliptical holes, where each corresponds to either an up or down movement of the chest. These holes can easily be detected and counted by persistent homology. The point cloud is similar to the original time-series signal in Fig. 2 but with additional samples that are equally spaced on the baseline level. Moreover, the point cloud lies in a 2-D Euclidean space. That is, coordinates of the points have no physical meaning; they only define a relative distance between any two points.

B. Persistent Homology

Homology is a TDA tool which enables us to infer topological features, such as components, holes, and voids, from the samples of geometric objects. A topological space can be approximated by a set of combinatorial objects called simplicial complexes. A simplicial complex is built from vertices, edges, triangular faces, and higher dimensional analogues, called simplices; a point is a 0-D simplex, an edge between two points is a 1-D simplex, a triangular face is a 2-D simplex, and so on. If the intersection of any two simplices is also a simplex, then they together form a simplicial complex. Once the space in which the point cloud resides is mapped into simplicial complexes, the underlying topology can be analyzed by applying homology. Homology counts the number of connected components, holes, and other high-dimensional surfaces so that can classify topologically equivalent spaces. In this letter, we use homology to count the number of semi-elliptical holes and later determine the RR.

1) Building Simplicial Complexes: Construction of simplicial complexes by treating all the members of a point cloud as vertices is computationally expensive. Therefore, we first consider reducing its size. There are two standard methods for subsampling a point cloud Z to a set of vertices, called landmark points, $L \subset Z$: random selection and maxmin algorithm [20]. Three hundred landmark points sampled from the point cloud (of 3200 points) in Fig. 4 are shown in Fig. 5. Landmarks selected by the maxmin method tend to cover the dataset and to be more evenly spaced. However, both methods turn out not to be suitable for our problem as many hole structures are lost in both cases. We thereby propose another technique. First, the original time-series signal is downsampled. Let $x_d(n)$ be the downsampled signal of $M \ll N$ points and μ be the mean value again. We then insert μ-valued samples between each pair of samples of $x_d(n)$ and form a point-cloud

$$L = [x'_d \quad t] \tag{4}$$

where $x'_d = [x_d(0), \mu, x_d(1), \ldots, x_d(M-2), \mu, x_d(M-1)]^T$, and $t = [0, 1, \ldots, 2M-1]^T$. Number of points in L can be reduced more by inserting μ values into the x_d vector less frequently, that is, after each k samples, where $k > 1$. The point cloud constructed with a downsampling factor of 12 and $k = 6$ is depicted in Fig. 6(a). Note that even though the total number of points is now half of those in the point clouds reduced by the random and maxmin methods, true topology is preserved.

Next step is to express the reduced point cloud L in terms of simplicial complexes. The most general way to construct them is to choose a scale parameter r and draw balls of radius $r/2$ around each points. If any two points $\{l_i, l_j\} \in L$ are no further apart than r, that is, the Euclidean balls $B(l_i, r/2)$ and $B(l_j, r/2)$ have nonempty intersection, then these points are connected with an edge. If there exits three points that are pairwise connected to form a triangle, then the triangle is filled in with a 2-D face. When all the complete simplices are filled in similarly, we obtain the Vietoris–Rips complex [21]. It can be denoted by $VR(L, r)$, where L is the set of vertices and r is the scale parameter. $VR(L, r)$ for $r = 6$ is shown in Fig. 6(b). As r is increased beyond that value; opposing points which enclose a hole get connected, new triangular faces are filled in, holes get smaller, and eventually all the subcomplexes join into a single huge complex.

2) Counting the Holes: Homology provides a way of summarizing the topological structure of a space in the form of so-called Betti numbers. β_k gives the number of k-dimensional holes, for example, β_0 is the number of connected components, β_1 is the number holes, β_2 is the number of voids, and so on [21]. Since the goal here is to find the number of holes, we will be dealing only with the first Betti number, β_1. The problem is how to choose the scale parameter r. If it is too small, then homology detects many holes due to noise. On the other hand, if it is too large, then any two points get connected and we end up with a trivial homology. Hence, rather than a fixed value of r, a more useful knowledge of the space can be obtained by considering a

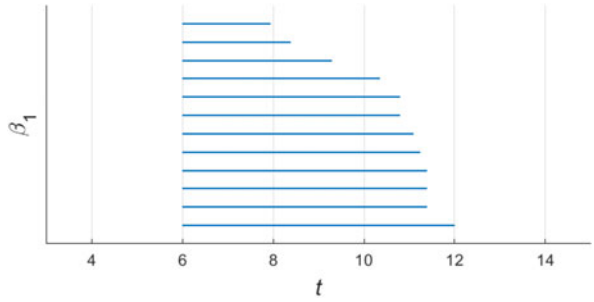

Fig. 7. Barcodes extracted from the complex in Fig. 6(b).

range of values. In this way, we obtain a sequence of simplicial complexes, called a filtration $VR(L,t)$, with the property that

$$VR(L,t_1) \subset VR(L,t_2), \quad t_1 < t_2. \tag{5}$$

That is, a simplicial complex constructed for a smaller scale parameter, which hereafter will be called as the filtration time, is a subset of the complex constructed for a larger one.

As we proceed through the filtration time, vertices get connected and holes start to appear. Each hole then disappears after a particular time as the subcomplexes become gradually connected. Persistence of a hole can be represented as a pair (t_i, t_f) which is referred to as Betti or persistence interval. We are interested in the persistence intervals that last for a long period of filtration time because they correspond to the holes larger in size, that is, the features. Small holes, which correspond to noise, have short persistence intervals because they are quickly filled in. Based on this observation, we can easily distinguish between a feature and noise.

Each persistence interval can be visualized as a bar covering the lifetime of the corresponding hole. The collection of bars is called the barcode. The barcode extracted from the reduced point cloud L for the first Betti number is depicted in Fig. 7. β_1 at a time t is the number of bars that cross the vertical line at time t. For example, at filtration time $t = 6$ in Fig. 7, β_1 is equal to 12. This is exactly the same number of chest movements captured by the PIR sensor. Since a breathing activity consists of a pair of up and down movements of the chest, RR can be determined by dividing β_1 to $2T$, where T is the length of the signal frame in minutes. Note that if the case was of a perfectly periodic signal, each persistence interval would span the same filtration period. In our case, holes appear almost at the same time due to proper subsampling of the point clouds, but die at different times because each hole has different sizes.

IV. Experiments and Results

To make comparisons between the proposed method and time-frequency techniques, sensor data were windowed in 1 min intervals. RR was determined from the PIR sensor which generates the greatest peak-to-peak voltage, that is, has a better view of the chest. Point-clouds were constructed by using the technique described in Section III-A and subsampled to reduce the amount of data by 90%. Javaplex library [22] was utilized to compute persistent homology. Inputs to the function provided by this library are: point cloud data, maximum dimension in which the persistent homology will be computed, maximum filtration time, and number of time divisions. The larger the values of the maximum filtration time and number of divisions, the higher the computational complexity. On the other hand, they should be selected large enough to capture the dominant features.

TABLE I
Performance Assessment of Methods for Estimation of RR Over 300 Test Signals for Each Lying Position

Method	MAE*		
	Supine	Prone	Side-lying
Proposed	0.29	0.66	0.37
AMDF [16]	0.41	1.86	0.69
ACF	0.56	1.31	0.52
FT	0.38	1.73	0.60
LED	0.71	1.64	0.66

*Unit in bpm.

Start-time and lifetime of the Betti intervals were trained to differentiate between true features and noise-related features. The Betti intervals which start within the specified time frame and persist longer than a threshold value T were counted and the number was divided by 2 to determine the RR on a per minute basis. Ten subjects that are not associated with a respiratory disorder were asked to lie in a bed in different positions, that is, supine, prone, and side-lying positions, and breathe normally for a minute. We considered 300 test signals in total for each position. RR of the subjects were annotated manually. Performance was assessed by calculating the mean absolute error (MAE) in bpm, defined as

$$\text{MAE} = \frac{1}{n}\sum_{i=1}^{n} |\widehat{\text{RR}_i} - \text{RR}_{\text{ref},i}| \tag{6}$$

where n is the number of tests, $\widehat{\text{RR}_i}$ is the estimated RR, and $\text{RR}_{\text{ref},i}$ is the reference RR for test i. We compared the error to that of produced by autocorrelation function (ACF) maximization, Fourier transform (FT), local extrema detection (LED), and the average magnitude difference function (AMDF) method [16]. Results are presented in Table I. Our method shows an excellent agreement with the ground truth with an average MAE of 0.44 and gives the best results in every lying position. Moreover, it does not require a long signal sequence unlike the AMDF, ACF, and FT methods to estimate the RR. LED may also be regarded as an online method but its performance worsens noticeably as the number of missing samples increases. On the other hand, the performance of the proposed method does not change due to subsampling of ratios up to 1/10.

V. Conclusion

In this study, we introduced the application of persistent homology to 2-D point clouds for the online estimation of period of signals oscillatory in nature but not strictly periodic. We demonstrated that it is possible to make reliable estimates of the RR from a PIR sensor array. The way that the point clouds are constructed enables us to preserve the period information of the original sensor signals. The proposed method requires only a limited number of data samples making the system implementable on a low-cost digital signal processor.

REFERENCES

[1] I. Trajkovic, C. Reller, M. Wolf, and H.-A. Loeliger, "Modelling and filtering almost periodic signals by time-varying fourier series with application to near-infrared spectroscopy," in *Proc. 17th Eur. Signal Process. Conf.*, 2009, pp. 632–636.

[2] B. M. Levitan and V. V. Zhikov, *Almost Periodic Functions and Differential Equations*. Cambridge, U.K.: CUP Archive, 1982.

[3] H. Krim, T. Gentimis, and H. Chintakunta, "Discovering the whole by the coarse: A topological paradigm for data analysis," *IEEE Signal Process. Mag.*, vol. 33, no. 2, pp. 95–104, Mar. 2016.

[4] G. Tabak and A. C. Singer, "Non-contact heart rate detection via periodic signal detection methods," in *Proc. 2015 49th Asilomar Conf. Signals, Syst. Comput.*, 2015, pp. 790–794.

[5] S. Emrani, T. Gentimis, and H. Krim, "Persistent homology of delay embeddings and its application to wheeze detection," *IEEE Signal Process. Lett.*, vol. 21, no. 4, pp. 459–463, Apr. 2014.

[6] H. L. Yap and C. J. Rozell, "Stable takens' embeddings for linear dynamical systems," *IEEE Trans. Signal Process.*, vol. 59, no. 10, pp. 4781–4794, Oct. 2011.

[7] F. Erden and A. E. Cetin, "Breathing detection based on the topological features of IR sensor and accelerometer signals," in *Proc. 2016 50th Asilomar Conf. Signals, Syst. Comput.*, 2016, pp. 1763–1767.

[8] S. Emrani and H. Krim, "Spectral estimation in highly transient data," in *Proc. 23rd Eur. Signal Process. Conf.*, 2015, pp. 1721–1725.

[9] I. Homma and Y. Masaoka, "Breathing rhythms and emotions," *Exp. Physiol.*, vol. 93, no. 9, pp. 1011–1021, 2008.

[10] S. D. Min, Y. Yun, and H. Shin, "Simplified structural textile respiration sensor based on capacitive pressure sensing method," *IEEE Sensors J.*, vol. 14, no. 9, pp. 3245–3251, Sep. 2014.

[11] B. Padasdao, E. Shahhaidar, C. Stickley, and O. Boric-Lubecke, "Electromagnetic biosensing of respiratory rate," *IEEE Sensors J.*, vol. 13, no. 11, pp. 4204–4211, Nov. 2013.

[12] X.-R. Ding, Y.-T. Zhang, H. K. Tsang, and W. Karlen, "A pulse transit time based fusion method for the noninvasive and continuous monitoring of respiratory rate," in *Proc. IEEE 38th Annu. Int. Conf. Eng. Med. Biol. Soc.*, 2016, pp. 4240–4243.

[13] D. Zito *et al.*, "SoC CMOS UWB pulse radar sensor for contactless respiratory rate monitoring," *IEEE Trans. Biomed. Eng.*, vol. 5, no. 6, pp. 503–510, Dec. 2011.

[14] Y. Kurihara and K. Watanabe, "Development of unconstrained heartbeat and respiration measurement system with pneumatic flow," *IEEE Trans. Biomed. Eng.*, vol. 6, no. 6, pp. 596–604, Dec. 2012.

[15] C. B. Pereira, X. Yu, V. Blazek, B. Venema, and S. Leonhardt, "Multisensor data fusion for enhanced respiratory rate estimation in thermal videos," in *Proc. IEEE 38th Annu. Int. Conf. Eng. Med. Biol. Soc.*, 2016, pp. 1381–1384.

[16] F. Erden, A. Z. Alkar, and A. E. Cetin, "Contact-free measurement of respiratory rate using infrared and vibration sensors," *Infrared Phys. Technol.*, vol. 73, pp. 88–94, 2015.

[17] F. Erden *et al.*, "Wavelet based flickering flame detector using differential pir sensors," *Fire Safety J.*, vol. 53, pp. 13–18, 2012.

[18] H.-T. Chu and T.-C. Fu, "Analysis of exercise ventilation with autoregressive model and hilbert-huang transform," in *Proc. Int. Comput. Symp.*, 2015, vol. 274, pp. 185–192.

[19] F. Takens, "Detecting strange attractors in turbulence," in *Dynamical Systems and Turbulence*. New York, NY, USA: Springer, 1981, pp. 366–381.

[20] V. De Silva and G. Carlsson, "Topological estimation using witness complexes," in *Proc. Symp. Point-Based Graphics*, 2004, pp. 157–166.

[21] G. Carlsson, "Topology and data," *Bull. Amer. Math. Soc.*, vol. 46, no. 2, pp. 255–308, 2009.

[22] A. Tausz, M. Vejdemo-Johansson, and H. Adams, "JavaPlex: A research software package for persistent (co)homology," in *Proc. 4th Int. Conf. Math. Softw.*, 2014, pp. 129–136. [Online]. Available: http://appliedtopology.github.io/javaplex/.